Journal of Alzheimer's Disease 42 (2014) 1279–1294
DOI 10.3233/JAD-140672
IOS Press

Fibroblast Aggregation Rate Converges with Validated Peripheral Biomarkers for Alzheimer's Disease

Florin V. Chirila*, Tapan K. Khan and Daniel L. Alkon
Blanchette Rockefeller Neurosciences Institute, Morgantown, WV, USA

Accepted 8 May 2014

Abstract. The inaccuracy of the diagnosis for Alzheimer's disease (AD) has made its therapeutic intervention difficult, particularly early enough to prevent significant neurodegeneration and cognitive dysfunction. Here, we describe a novel, highly accurate peripheral diagnostic for AD patients based on quantitatively measured aggregation rate of human skin fibroblasts. The elevated aggregation rate with increasing cell density in AD cases is the basis of this new biomarker. The new biomarker was successfully cross-validated with two more mature assays, AD-Index, based on the imbalances of ERK1/2, and Morphology, based on network dynamics, and showed 92% overlap. A significant number of cases tested with this new biomarker were freshly obtained ($n = 29$), and 82% of the cases are hyper-validated cases, i.e., autopsy and/or genetically confirmed AD or non-Alzheimer's disease demented patients (Non-ADD) and non-demented age-matched controls. Furthermore, we show that by using a simple majority rule, i.e., two out of the three assays have the same outcome, we significantly increase the agreement with clinical AD diagnosis (100%). Based on the high accuracy of this strategy, the biomarker profile appears to accurately identify AD patients for therapeutic intervention.

Keywords: Aggregation rate, Alzheimer's disease, cross-validation, majority rule, skin fibroblasts

INTRODUCTION

We have developed three independent peripheral diagnostic assays for Alzheimer's disease (AD) using skin fibroblasts; AD-Index [1–4], Morphology [5], and PKCε, which were previously tested with 139 cases out of which more than 80% were hyper-validated cases, i.e., autopsy and/or genetically confirmed AD or non-Alzheimer's disease demented patients (Non-ADD) and non-demented age-matched controls (AC). One of these three assays, the morphology assay, is based on abnormal aggregation of skin fibroblasts harvested from AD patients.

Fibroblast aggregation is correlated with intercellular adhesiveness [6]. In disease cases, the adhesiveness of fibroblasts is abnormal. For example in Duchenne muscular dystrophy (DMD), fibroblast adhesiveness is reduced to 40% from that of normal cells [6], while fibroblasts from fetal Down syndrome show an increased adhesiveness, therefore increased aggregation [7]. In the case of Down syndrome, the increase adhesiveness of lung and cardiac fibroblasts during organogenesis could explain malformations such as pulmonary hypoplasia and congenital heart defects [7]. Down syndrome patients who live long enough will develop AD. Therefore an abnormal fibroblast aggregation is expected and was reported in AD patients [5].

A systematic analysis of fibroblast aggregation in DMD patients revealed that a small subpopulation of cells is very adhesive and formed a small number of large aggregates [8]. The large fibroblast aggregates specific to DMD were not present in age-matched controls and were correlated to intercellular adhesiveness [8]. In our previous studies of human dermal fibroblast aggregation [5], we also observed large aggregates for AD patients when compared with age-matched controls for which the cellular aggregation was more

*Correspondence to: Florin V. Chirila, Blanchette Rockefeller Neurosciences Institute, 8 Medical Center Drive, Morgantown, WV 26506, USA. Tel.: +1 304 293 8404; Fax: +1 304 293 3675; E-mail: fchirila@brni.org.

ISSN 1387-2877/14/$27.50

evenly distributed. We quantified cell aggregation by the area of the unit aggregate, which is the average area per number of aggregates (A/N) at 48 hours, after plating on Matrigel.

The complex kinetics of normal and transformed BHK21 fibroblast aggregation in shaking suspension suggests that the polyoma-transformed fibroblasts have a lower adhesiveness [9]. Furthermore the light trypsin/EDTA treatment produced an opposite kinetic of aggregation when compared with the heavy trypsin/EDTA treatment [9].

One interesting hypothesis arising from colloidal science suggests that the initial particle size distribution of coagulating hydrosols tend to preserve their shape [10]. Similarly in the field of cell biology, it has been suggested that if the initial cell size and shape is different in normal versus transformed/diseased cells, this difference tends to be conserved during cellular aggregation [9]. More interestingly, it has been suggested that the built-in differences in cell morphology population will result in differences in aggregation kinetics [9].

Human dermal fibroblast aggregation on Matrigel was studied in comparison with human umbilical vein endothelial cells [11], and it has been shown that both types of cells aggregate and form cord networks which mimic only partially an angiogenic phenomenon. We previously reported that these spatiotemporal networks have a different dynamic in skin fibroblast from AD patients when compared with skin fibroblasts from age-matched controls [5]. It has been reported that Matrigel stimulate differentiation of Sertoli cells [12] and mouse kidney cells [13].

The aggregates of human dermal fibroblasts were constructed on purpose in rotational shaking with non-treated dishes to accelerate wound healing [14, 15]. The aggregate formation was enhanced by the medium supplements such as insulin, dexamethasone, ascorbic acid, and basic fibroblast growth factors, which potentiate secretion of extracellular matrices, and promote cell-cell interaction [14, 15]. The working hypothesis is that high density cell aggregates increase cell-cell interaction and therefore increase the probability of further accelerating skin wound healing [8, 9]. Interestingly, these studies too pointed that the lack of aggregation is due to high adhesiveness of fibroblasts, indicating that by reducing the adhesiveness by using plastic dishes for non-adhesive cells the aggregation increased.

The increased cellular aggregation due to reduced adhesiveness was also reported for diseased cells from DMD [6] or AD [5]. Furthermore, increased cellular aggregation is promoted by increasing cell-cell interaction when adding medium supplements such as insulin, dexamethasone, ascorbic acid, and basic fibroblast growth factors [14, 15] or by adding of water-soluble conjugates of cell adhesion peptides containing a sequence of three amino acids, Arg-Gly-Asp (RGD), and poly (ethyleneglycol) (PEG) [16].

Here we report an elevated aggregation rate with increasing cell density in fibroblasts from AD patients when compared with AC and Non-ADD patients. Furthermore, we suggest that the rate of aggregation could be used as a new biomarker for screening AD patients.

Analysis of 38 cases, with 9 banked (Supplementary Table 1) and 29 (Supplementary Table 2) cases from the clinic, suggest a clear separation between AD and AC/Non-ADD when using the aggregation rate as a biomarker.

The analysis of the probability distributions of the slope and intercept for 35 samples suggests that the probability distribution for the AC group ($n = 27$) is narrower and resides on the tail of the probability distribution of the AD group ($n = 8$) which is wider. This indicates that for larger data sets the estimated overlapping probability for the two groups, AD and AC, is less than 10%.

Table 1
Possible states for the sum of the normalized values of the three biomarkers by the cutoff values. U, uncertain state which is when the value of the biomarker is equal with the cutoff value

Aggregation Rate	AD-Index	Aggregation Area per Number	Sum	Diagnosis
1	1	1	3	AD
1	1	U*	2	AD
1	1	-1	1	AD
1	-1	-1	-1	AC/Non-ADD
-1	-1	U*	-2	AC/Non-ADD
-1	-1	-1	-3	AC/Non-ADD
+/-1	U	U**	2U	Not diagnosed
U	U	U	3U	Not diagnosed

*Here we refer to a situation where we have one uncertain biomarker out of the three. **Here we refer to a situation where we have two uncertain biomarkers out of the three. By this measure, S, there are three states: 1) AD for S = 1, 2,3 in green; 2) AC/Non-ADD for S = -1,-2,-3 in red; and 3) Not diagnosed for two (2U) or three (3U) uncertain i.e., cutoff values, in black. Similarly a simple Excel function, count if can be used to count the positive values, +1, or the negative values, −1. If the result of the count if for the +1 are >=2 than that case is an AD. If the result of the count if for the +1 is <2 than that case is an AD/Non-ADD (Table 2). If the case has two or more uncertain (U), i.e., cutoff values than that case cannot be diagnosed. Similarly the count can be done for the −1 values but this will be just redundant.

Table 2
Possible states for the count if (>0/<0) of the normalized values of the three biomarkers by the cutoff values

Aggregation Rate	AD-Index	Aggregation Area per Number	Count if >0	Count if <0 (redundant)	Diagnosis
1	1	1	3	0	AD
1	1	U	2	0	AD
1	1	-1	2	1	AD
1	-1	-1	1	2	AC/Non-ADD
-1	-1	U	0	2	AC/Non-ADD
-1	-1	-1	0	3	AC/Non-ADD
+/-1	U	U	NA	NA	Not diagnosed
U	U	U	NA	NA	Not diagnosed

U = uncertain state which is when the value of the biomarker is equal with the cutoff value. By this measure, sum of the binary values, there are three states: 1) AD for count if (>0) = 2, 3 in green; 2) AC/Non-ADD for count if (>0) = 0, 1 in red; and 3)Not diagnosed for two or more uncertain, i.e., cutoff values in black. The results for the count if (>0), gray background in Table 2 are shown in the Fig. 8C, D.

The trend of higher rate of change of cell aggregation for AD cases when compared with AC/Non-ADD cases is in line with our previous studies in which we reported that AD cells are consistently bigger and less adhesive in average, than the AC/Non-ADD cells.

The new biomarker quantifying the aggregation rate was cross-validated with the two more mature assays, AD-Index, based on the imbalance of ERK1/2, and Morphology, based on network dynamics (A/N). The cross-validation resulted in 92% overlap with each of the two assays.

Furthermore, we report here that a simple majority rule, i.e., two out of the three assays give the same outcome, increases the agreement with clinical diagnosis to 100%.

MATERIALS AND METHODS

Banked and fresh cell lines used in this study

We carried out experiments using skin fibroblast samples from 38 patients, with 9 banked cases (See Supplementary Table 1) provided by the Coriell Institute for Medical Research (Camden, NJ), and 29 cases (See Supplementary Table 2) from the clinic provided by Marshall University (Huntington, WV). We plated the fibroblast on a thick layer (∼1.8 mm) of 3-D matrix (Matrigel, BD Biosciences, San Jose, CA) on 12 well plates [5]. The available patient information is posted on Coriell web site (http://ccr.coriell.org/). The cell lines analyzed ($n = 38$) were for the most part (29/38) from the clinic serving also as a validation for the previous studies with banked samples [5]. The age-matched control (AC) cases chosen for this paper were not demented at the date of skin biopsy extraction. All the samples were taken antemortem. The banked skin fibroblast cells were frozen stocks under liquid nitrogen. Primary cultures were established after thawing those frozen samples and followed through successive passaging [1–5]. All cell lines used in this study were primary cell lines and were not treated in order to be immortalized.

Freshly taken fibroblasts were obtained as follows. Punch-biopsies (2-3 mm, upper arm) of skin tissues from patients and controls were obtained by qualified personnel under the supervision of Dr. Shirley Neitch with the IRB approval of Marshall University (Huntington, WV). All patients (or relatives/representatives) signed informed consent forms. The clinical diagnosis was conducted by Dr. Neitch. The Institutional Review Board at Marshall University approved the procedure. The method of isolating fibroblasts from skin biopsies was followed as described elsewhere [1]. For the tests described here, we used cells with passages between 5 and 15.

The initial cell density was controlled to be 50 cells/mm^3 and was homogenized with 1.5 ml Dulbecco Modified Eagle Medium with 10% fetal bovine serum and 1% penicillin/streptomycin for each well. Cells were kept in a CO_2 water-jacket incubator (Forma Scientific) up to 7 days after plating.

Image capture

Images of the cellular networks were captured with an inverted microscope (Westover Digital AMID Model 2000, Westover Scientific, Bothell WA), controlled by a computer via an image acquisition software (Micron 2.0.0), using a 10× and a 4× objective. We

captured five to nine images per well and typically we used four wells per cell line. In the first day we acquired images at 30 min after seeding, the second day at 24 h, and the third day at 48 h. Images were processed with ImageJ, a freely available software from NIH (http://rsbweb.nih.gov/ij/).

The 5 images per well were initially taken using the same standard pattern, center (1), up (2), down (3), left (4), right (5), by moving one image field with respect to the central image [5]. Later in the process, we increased the number of images from 5 to 9 by filling the corners of the rectangle with images from 6 to 9 [5], in order to increase the area investigated and further improve the coefficient of variation without affecting the diagnostic discriminability. Image 1 was always in the center of the well. To determine the center of the well we used one of the following methods: a) the live image under 4× magnification should be symmetric, i.e., the shadows in the four corners should have equal areas for an aligned microscope; b) mark the center with a needle; or c) use gridded plates (Pioneer Scientific; Shrewsbury, MA) where the central square is always the 6th, in the central row or column. For image quantification we used two sets of tools: initially manual as provided by Micron, software which came with the microscope; later automated with ImageJ.

For the initial cell count, we used a custom ImageJ plug-in in which we ran "despeckle" three times; we then filtered the image three times with a minimum filter of radius 0.5; and then we ran "Subtract Background" with a rolling radius of 20. Finally, we made the image binary and ran "Analyze Particles" in the size range 200–10000. All of these ImageJ commands were run inside a loop so that we could analyze all the images from one cell line automatically. The ImageJ plug-in was tuned by using manual cell counts on the same images and the relative error was below 7%.

The target number of cells per 10× image was 417 which corresponded to an initial cell concentration of 50 cells/ml [11]. We allowed a variation of cell concentration between 45 and 60 cells/ml. To minimize heterogeneity of the cell distribution in the image, we eliminated images outside of the range 320–550 cells per 10× image. For cellular aggregates at 48 h we used manual ellipse fitting with the Micron software.

Average area per number of aggregates (A/N)

A/N was calculated in the following manner. For each image, i.e., we calculate an average aggregate area,<A>i, and counted the number of aggregates, Ni. Then for each image we evaluate the ratio < A>i/Ni. Typically, we used nine images per well and we evaluate an average area per number for each well as the $\langle \langle A \rangle_i / N_i \rangle = \frac{1}{9} \sum_{i=1}^{9} \frac{\langle A \rangle_i}{N_i}$. Then we average once more over the four wells $\langle \langle \langle A \rangle_i / N_i \rangle \rangle = \frac{1}{4} \sum_{w=1}^{4} \left(\frac{1}{9} \sum_{i=1}^{9} \frac{\langle A \rangle_i}{N_i} \right)_w$. For the purpose of simplifying the discussion we will use A/N instead of $\langle \langle \langle A \rangle_i / N_i \rangle \rangle$. The aggregates were manually fitted with ellipses using Micron 2.0 software and their area and number were recorded. We developed an automatic script for ImageJ which agrees well with manual ellipse fitting. These two approaches were within one standard deviation of each other. For simplicity we called A/N area of the unit aggregate.

Aggregation rate

Rather than calculating A/N which involves averaging across the four wells as described in the section above, we look at the dependence of A/N on cell density (Fig. 1A), and then fit this dependence with a line, f(x) = s*x+int. From the linear fit, we analyzed the slope(s) and intercept (int) for the population of 38 cases. The linear fit was done within the boundaries 320 to 550 cells per 10× image field. For the aggregation rate, we have only single experiments where the cell density varies between 320 to 550 cells per 10× image. Therefore for this data set, we cannot report the standard error of the mean. However, we are reporting in Fig. 9 the test-retest validation for the aggregation rate for 1 AC subject and 1 AD case.

Quantification of cross-validation

The three biomarker values were normalized between 0 and 1 as $\frac{(x-min)}{(max-min)}$, where x is the biomarker value to be normalized, max is the maximum value, and min is the minimum value of the data set of 26 cases. This normalization brings all the three biomarkers within the same range, 0 to 1, which makes the comparison easier (Fig. 8A).

The curve fitting for all three biomarker values was done in two steps. First the fitting was done with a linear function, f(x) = a*x+b, for the AC values and with an exponential function, g(x) = c*exp(d*x), for the AD values. Second fit was done with a glued function h(x) = f(x) + g(x) = a*x+b + c*exp(d*x). For the starting values of the parameters a, b, c, and d, we used the end values from the previous fit. After fitting with the glued function, h(x), the new fit parameters were recorded and used for the plots in Fig. 8A.

Cross-correlation of biomarkers

For assessing which pair of biomarkers is best correlated we used the absolute difference per case, $|b_1 - b_2|$, $|b_2 - b_3|$, and $|b_3 - b_1|$ where b_1 = AggR, b_2 = ADI, b_3 = A/N. The average values of the absolute differences were then calculated for all the 19 AC cases, $\langle (b_j - b_k) \rangle_{AC} = \frac{1}{19} \sum_{i=1}^{19} (b_j - b_k)_i$, where j, k = 1,3, and $j \neq k$, and all the 7 AD cases, $\langle (b_j - b_k) \rangle_{AD} = \frac{1}{7} \sum_{i=1}^{7} (b_j - b_k)_i$,where j, k = 1,3, and $j \neq k$. The overall averages for the absolute differences were also calculated for all 26 values, $\langle (b_j - b_k) \rangle_{AD} = \frac{1}{26} \sum_{i=1}^{26} (b_j - b_k)_i$. The smaller these group differences are the closer the two biomarkers are correlated Fig. 8B.

Quantification of the majority rule

For the quantification of the majority rule we normalized once more the biomarker values, x, with respect to the specific Cutoff value, $\frac{(x-Cutoff)}{|x-Cutoff|}$. Examples are shown in Fig. 8C and D with the colored vertical bars, for the 7 AC and 7 AD cases. There are three possible outcomes of this cutoff normalization -1, 1, and uncertain (U). When the biomarker value, x, is equal with the cutoff value, we have an uncertain situation, i.e., we cannot diagnose the case and we label the output of the biomarker as uncertain (U). This second normalization with respect to the cutoff value simplifies the outcome of the biomarker into three states: +1 for AD, −1 for AC and Non-ADD, and U for cutoff values. Then considering that we have three biomarkers, the possible states for the sum(S) will be {3, 2, 1,-1,-2,-3, 2U, 3U}.

Data analysis

For data analysis, we used Gnuplot 4.4, a freely available software (http://www.gnuplot.info). For fitting of the raw data points, we used a built in fit function from Gnuplot, which uses an implementation of the nonlinear least-squares (NLLS) Marquardt-Levenberg algorithm. Unless otherwise specified, the error-bars are standard errors of the mean (SEM).

Probability distribution of cellular aggregates

For all the AD and all the AC patients, we binned the values for slope(s) and intercept (int) of aggregates into equal intervals, fit with Gaussian functions for each variable, and then integrated into a normalized two-dimensional distribution.

RESULTS

Increased AD Aggregation Rate for Banked Samples

Cell aggregation is enhanced in AD patients when compared with AC and non-ADD subjects [5]. Cell aggregation was quantified by the area of the unit aggregate, which is the A/N at 48 h, after plating on Matrigel. The abnormal fibroblast aggregation in AD cases [5] is in line with abnormal aggregation of fibroblast from other diseased cases such as DMD [6, 9] or Down syndrome [8]. Note that the average life expectancy for DMD is 25 years and therefore the probability of overlapping with sporadic AD, which typically occurs after 50 years of life, is minimal.

Here we look at a new way of screening AD patients from AC and non-ADD subjects based on increasing cell aggregation when the cell density increases which we call slope intercept representation of cell aggregation. The slope intercept representation for cell aggregation has an intrinsic value as a new biomarker and helps with further understanding the increased cell aggregation for AD cases. This new biomarker, is a more refined representation of cell aggregation than a simple average (A/N), and might be a useful tool of double checking the AD/AC/Non-ADD cases which are too close to the cut-off line in the A/N representation.

An example of the dependence of cell aggregation (A/N) on cell density (# cells/10× image field) is illustrated in Fig. 1A. The linear dependence for the three examples (1AD, 1 AC, and 1 Non-ADD) is illustrated by the fit lines (Fig. 1A). The AD slope (green) is a lot steeper than the AC (red) or Non-ADD (blue) slope, and, as a consequence, the AD intercept is a lot more negative than the intercept for AC and Non-ADD (Fig. 1A, B).

A small number of banked cases from Coriell (9 cell lines: 3AD, 3AC, and 3 Non-ADD) show the same separability between AD and the other two groups (Fig. 1B, C). The line fit was done in the window 320–550 cells per 10× image. A zoom in for the rectangle in Fig. 1B, presented in Fig. 1C, shows a gap both in the slope (∼30) and the intercept (15000), between the near cut-off AC case and the near cut-off AD case.

Furthermore, in this representation we also are able to confirm that AD/AC/Non-ADD separation increases for the 48-h time point when compared with the 24-h time point (Fig. 1D) [5]. The arrows indicate that for all 3 AD cases the slope is steeper and therefore the

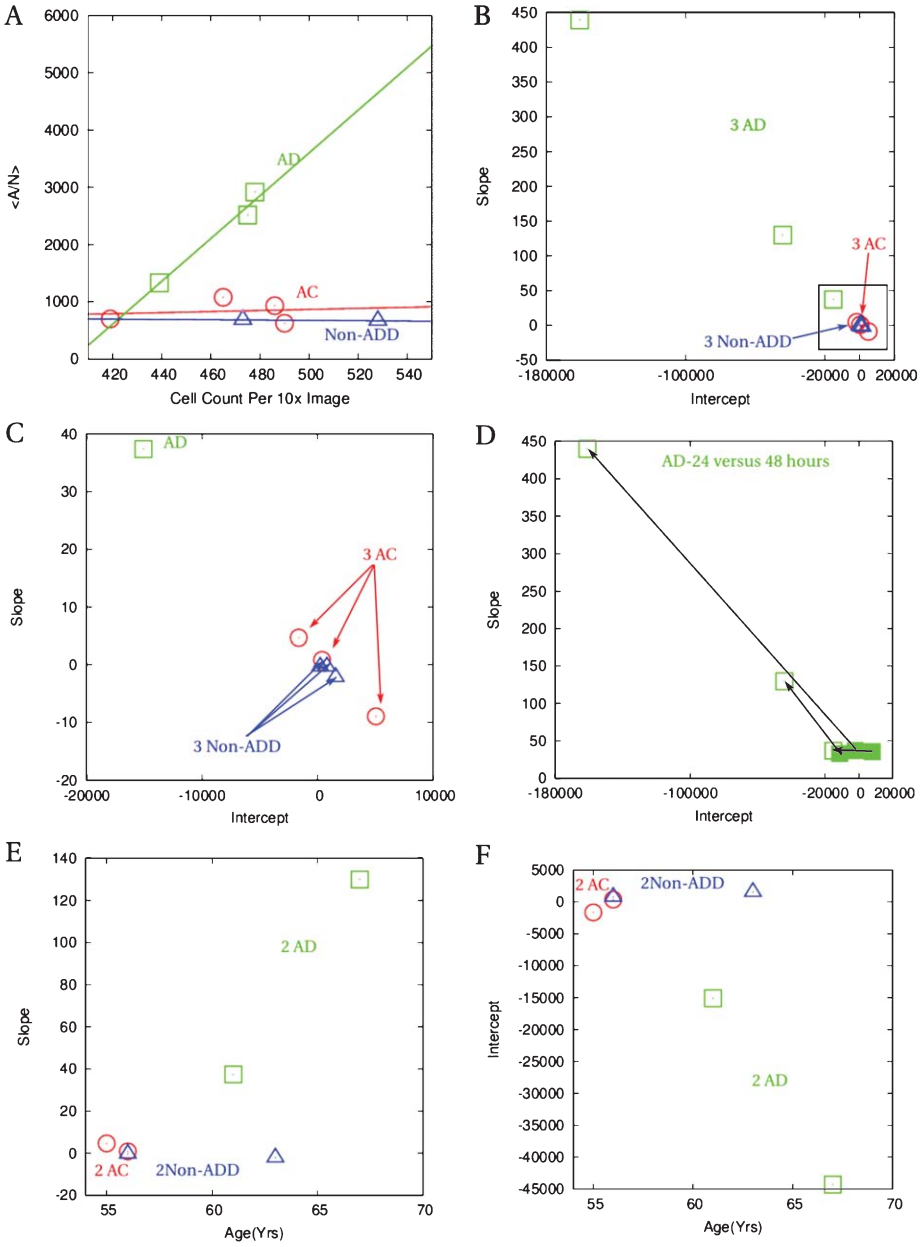

Fig. 1. Increased Alzheimer's disease (AD) aggregation rate for banked skin samples. A) Three examples of the dependence of area per number of aggregates (A/N) on the cell density (# cells/10× image field). The dependence was studied in the density range 320 to 550 cells per 10× image field. The AD cases are in green, the age-matched control (AC) cases are in red, and the non-Alzheimer's disease demented cases (Non-ADD) are shown in blue. B) The banked AD cases ($n = 3$) show a higher slope and a more negative intercept when compared with AC cases ($n = 3$) and Non-ADD cases ($n = 3$). C) A zoom in for the rectangle from panel B shows a significant gap in slope (~30) and intercept (15000) between the lowest AD case (green) and upper AC case (red). D) For the AD cases ($n = 3$), slope is steeper and intercept is more negative at 48 h (empty symbols) when compared with 24-h images (filled symbols). AC-red, AD-green, Non-ADD-blue. E) Slope dependence on age of the patient. 2 AD cases (green), 2 AC cases (red), and 2 Non-ADD cases (blue) are plotted in the age range 55 to 70 years. The AD cases show a higher aggregation rate in this age range. F) Dependence of the intercept on the age of the patient for the same cases as in panel E.

intercept goes more negative at 48 h when compared with 24-h time point. In other words, the AD cases move further away from the cut-off at 48 h when compared with 24 h, confirming that 48 h is an optimum time-point for this biomarker, which is consistent with our previous finding for A/N [5].

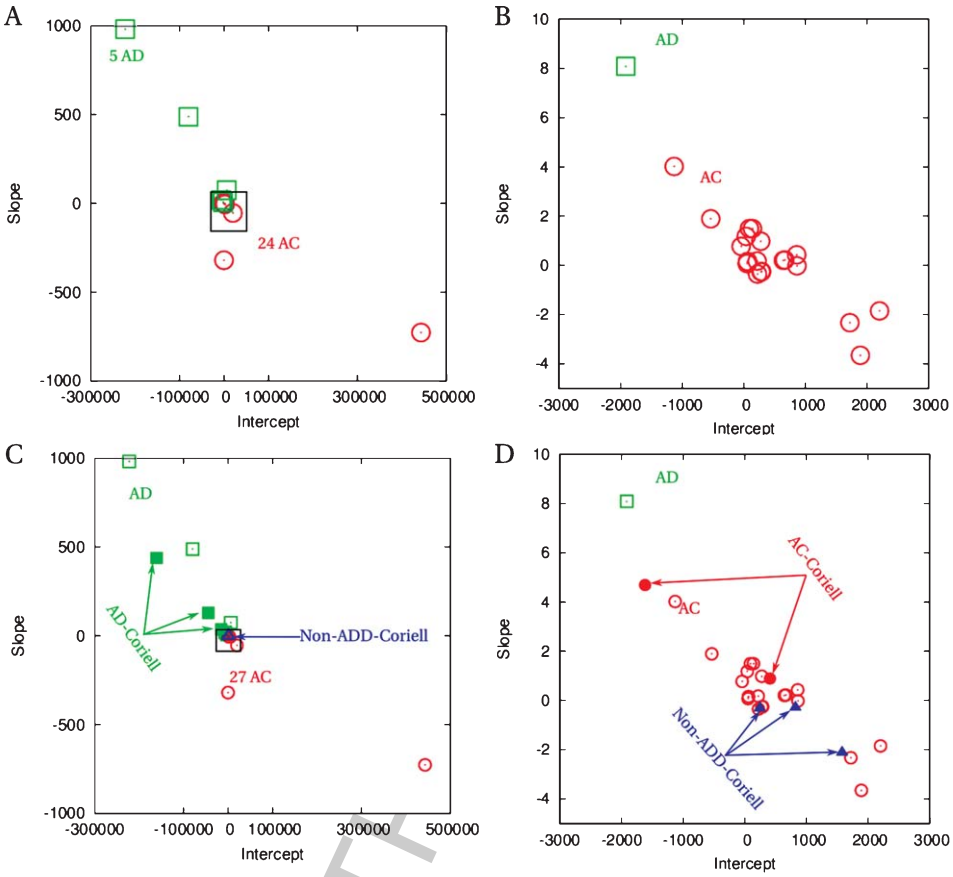

Fig. 2. Increased AD aggregation rate for samples from the clinic. A) Slope and intercept for 24 AC and 5 AD samples from the clinic. B) Zoom in near the cut-off (rectangle in panel A) reveals a gap in the slope (2) as well as in the intercept (500). C) Plots of banked Coriell (filled symbols) and fresh samples (empty symbols) from the clinic show similar trends and separation between AD and AC groups. D) Zoom in near the cut-off (rectangle in panel C). AC-red, AD-green, Non-ADD-blue.

The aggregation rate (slope) and intercept change with age as depicted in Fig. 1E and F, and, for approximately the same age-range (55–70 years), the AD cases show a higher aggregation rate. Previous studies of the dependence of cell aggregation (A/N) on age showed that the AD diagnostic discriminability is preserved in the age range of 50–90 years.

In summary, the slope/intercept analysis shows another way of screening AD cases from age-matched control cases and from Non-ADD patients. The slope intercept representation for cell aggregation is a more refined representation of cell aggregation than a simple average, i.e., A/N, and might be a useful tool to resolve the AD/AC/Non-ADD cases which are too close to the cut-off line in the A/N representation. Typically the cut-off line for the AD and AC populations is at the intersection of the two Gaussian distributions that fit the biomarker outputs. In a narrow region near the cut-off line, the tails of the Gaussian distributions coexist with certain probability therefore defining a gray zone of false positive/negative. Unknown cases falling in the gray zone for the A/N measure might be removed by using the rate of change of A/N.

Validation of increased AD aggregation rate with fresh samples from the clinic

The discrimination of AD cases from AC cases using the slope intercept analysis was further investigated in 29 samples from the clinic. Among these samples, 5 were AD cases and 24 were AC cases. The higher slope and more negative intercept for AD cases was confirmed by this study (Fig. 2A), as well as the gap between the AD and AC groups (Fig. 2B). The slope and intercept for banked samples from Coriell Cell Repositories and fresh samples are showing the same trend (Fig. 2C). The size of the gap in slope (∼2) and intercept (∼500) is also preserved when these two

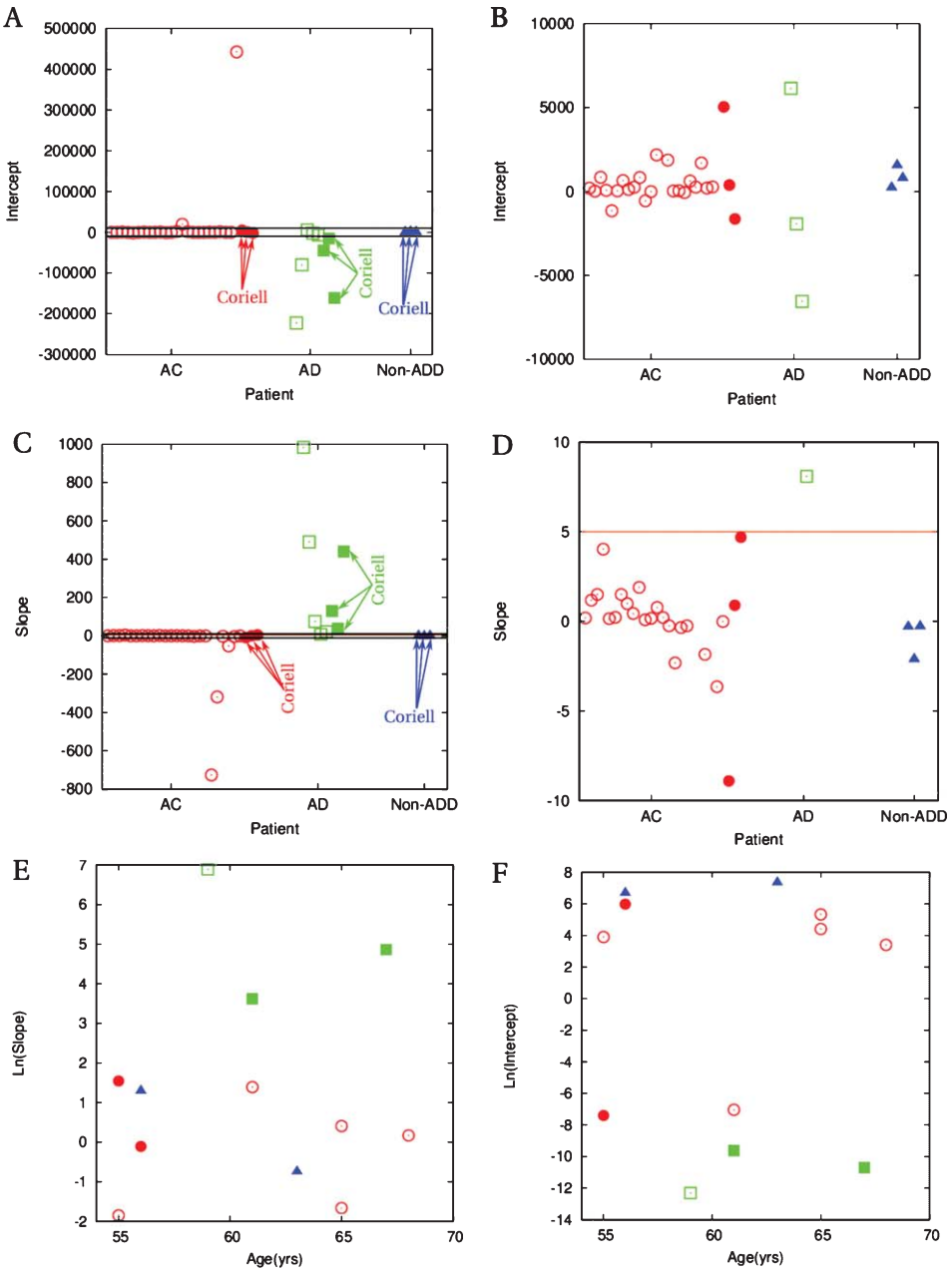

Fig. 3. Slope and intercept of A/N versus cell density. A) Intercept for 24 AC and 5 AD samples from the clinic (empty symbols) and 3 AC, 3 AD, and 3 Non-ADD banked samples from Coriell Cell Repositories (filled symbols). B) Zoom in near the cut-off (rectangle in panel A) reveals overlapping values in the intercept. C) Slope for the same samples from the clinic (24 AC and 5 AD; empty symbols) and the same banked samples (3 AC, 3AD, 3 Non-ADD; filled symbols). D) Zoom in near the cut-off locus (rectangle in panel C) reveals no overlapping values in the slope. AC-red, AD-green, Non-ADD-blue. E) Slope dependence on age of the patient. 3 AD cases (green), 7 AC cases (red), and 2 Non-ADD cases (blue) are plotted in the age range 55 to 70 years. The AD cases show a higher aggregation rate in this age range. F) Dependence of the intercept on the age of the patient for the same cases as in panel E.

data-sets are plotted (Fig. 2D). Narrowing of the gaps in slope and intercept is due to population increase from 9 cases from Coriell Cell Repositories, to 38 cases overall, which includes 29 samples from the clinic.

Aggregation rate drives the separation between the AD and AC groups

We further investigated what drives the separation between AD and AC groups, the slope or the inter-

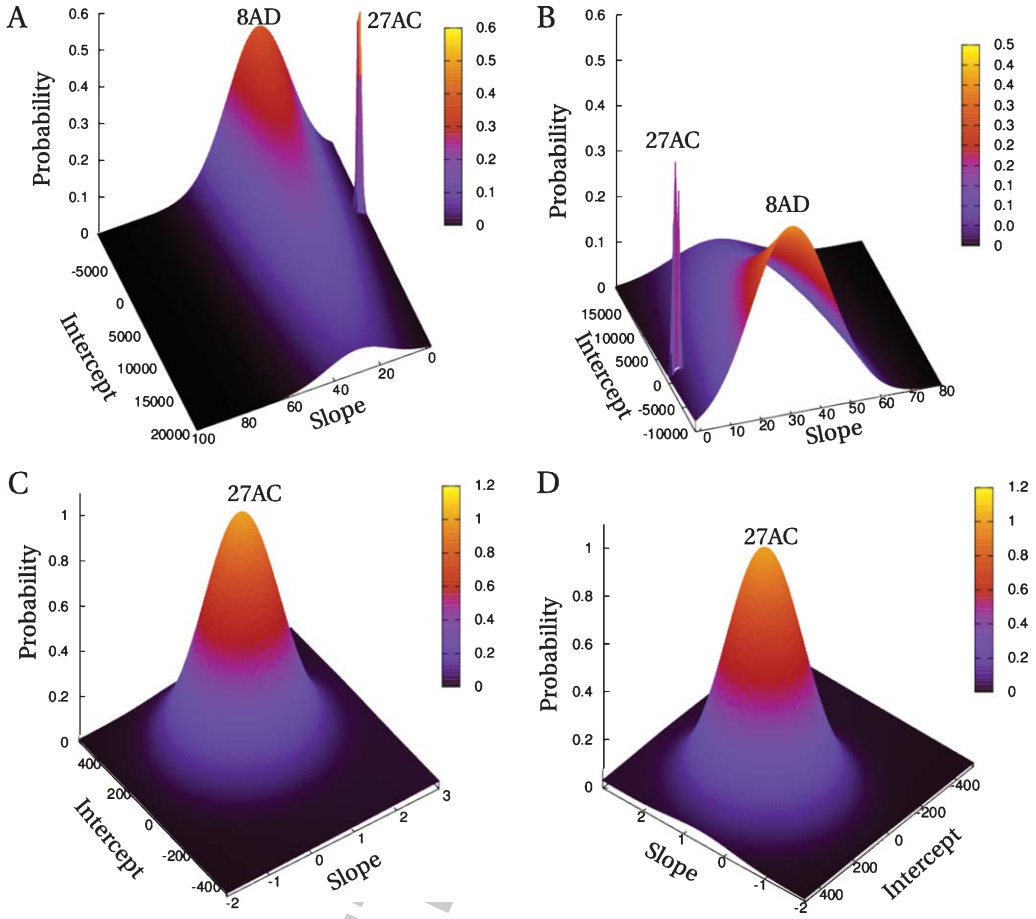

Fig. 4. Slope and intercept probability distributions. A) Probability distributions for 8 Alzheimer's disease (AD) patients and for 27 age-matched controls. B) Another view for the probability distributions for 8 AD patients and for 27 Age-matched controls (AC). C) Probability distribution for the 27 AC subjects reveals that an overlapping probability with the AD group is possible for larger data sets, and it is less than 10%. D) Another view for the probability distribution for 27 AC enforces the small overlapping probability with the AD group.

cept of A/N versus the cell density. For the purpose of achieving a greater separation between the AD and AC groups, we decided to analyze the slope and intercept independently. When we look at the intercept for the AC, AD. and Non-ADD groups both at large scale (Fig. 3A) as well as when we zoomed in near the cut-off locus (Fig. 3B), we noticed an overlap. This overlap will make this variable unsuitable for usage as an AD discriminator.

However the slope, i.e., the rate of change, shows a distinct separation between AD and AC/Non-ADD groups (Fig. 3C, D). So, the driving force of the separation we see between the AD and AC/Non-ADD groups is the rate of change of cell aggregation with increasing cell density.

As previously shown in Fig. 1E and F, the aggregation rate (slope) and intercept change with age as depicted in Fig. 3E and F, and for approximately the same age-range, 55–70 years, the AD cases show higher aggregation rate. The intercept is more negative for the AD cases than for the AC and Non-ADD cases. Please note that in Fig. 3E and F, we represented the natural logarithm of the actual values and in order to show negative values we used -ln(-negative values).

Slope and intercept probability distributions

The value of an AD biomarker can be assessed by using the probability distributions for the two groups, AD and AC. Based on these probability distributions, one can estimate the extent of possible overlapping probability when the data sets increase. The two groups of data (8 AD and 27 AC) were binned in slope and intercept. The probability distributions were estimated based on the frequency of occurrence in each bin divided by the total number of occurrences. The

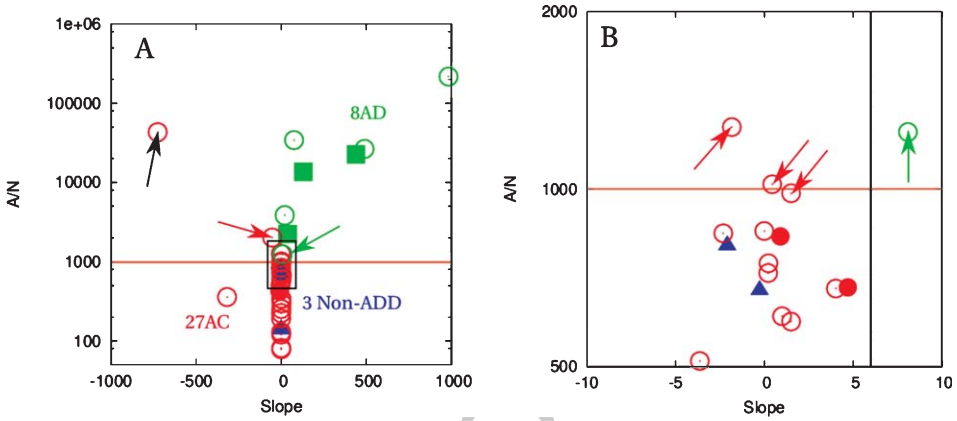

Fig. 5. Average area of the unit aggregate (A/N) versus aggregation rate (slope). A) A/N versus slope for 38 cases, 8 AD (green), 27 AC (red), and 3 Non-ADD (blue) cases. Filled symbols are banked samples from Coriell Cell Repositories, and empty symbols are fresh samples from the clinic. Black arrow indicates an AC case which is an outlier in the A/N representation but it is screened out correctly in the slope representation. Red/green arrows indicate AC/AD cases too close to the cut-off line in the A/N representation but are screened out correctly in the slope representation. B) Zoom-in for the rectangle from panel B reveals that the 3 AC (red arrows) and 1AD (green arrow) cases which are too close to the cut-off line in the A/N representation are screened out correctly in the slope representation.

raw probability data sets were fitted with Gaussian curves in variable, slope, and intercept. Then the two dimensional Gaussian probabilities were plotted using Gnuplot, a freely available software. The AC probability distribution is narrower than the AD probability distribution (Fig. 4A, B). The AC probability distribution resides on the tail of the AD probability distribution (Fig. 4C, D) which accounts for a slight upward shift (<10%) in the baseline. This upward shift is also the overlapping probability which is <10%. Although the data from 27 AC and 8 AD cases are not overlapping at all in the slope variable, this analysis suggests a possible overlapping for larger data sets. When using this variable as a biomarker for larger data sets, the estimated overlapping probability is less than 10%.

Average area per number of aggregates versus the aggregation rate

Previously we quantified the fibroblast aggregation as the A/N and reported an abnormally high aggregation in AD cases [5]. This time we further refined the measure, and find that the rate of change of A/N within cell density, within the boundaries 320 to 550 cells/10× image-field, is linear. Furthermore, we found that the aggregation rate (slope) is abnormally high for AD and it is the driving force for this biomarker.

In this section we show that the refined measure of cell aggregation, i.e., aggregation rate, works better than an average measure, i.e. A/N, which we previously defined [5] (also see the Methods section).

We looked at the population of 38 cases (8AD, 27 AC, and 3 Non-ADD) from the point of view of the efficacy of the two biomarkers quantified by the average area of the unit aggregate (A/N) and aggregation rate (slope). The A/N measure of cell aggregation is plotted against the aggregation rate (slope) in Fig. 5. In the A/N representation (y axis), we marked one AC case as an outlier (Fig. 5A, black arrow), because it is above the red horizontal line which is the cut-off line (A/N = 1000). The zoom in of the rectangular area from Fig. 5A reveals that 3 AC cases and 1 AD case (Fig. 5B) are too close to the cut-off line. Therefore, in this population of 38 cases, 5 cases are uncertain in the A/N representation with 1 case as an outlier and 4 cases too close to the cut-off line (gray zone). Five cases out of 38 represent 13% of the whole population which is a significant number when dealing with AD diagnosis. However, when we use the aggregation rate representation (x axis) of the cell aggregation, the uncertainty for the 5 cases is removed. The 4 AC cases are on the left side of the vertical cut off line, and one AD case is at the right side of the vertical cut-off line (Fig. 5B), therefore diagnosed the same as the clinical diagnosis.

In summary, when using the same experiment but a more rigorous analysis of cell aggregation, i.e., the aggregation rate (slope), we screened all of the 38 cases correctly. Therefore the rate of change of cell aggregation with increasing cell density becomes a powerful tool for checking the less sophisticated measure of A/N.

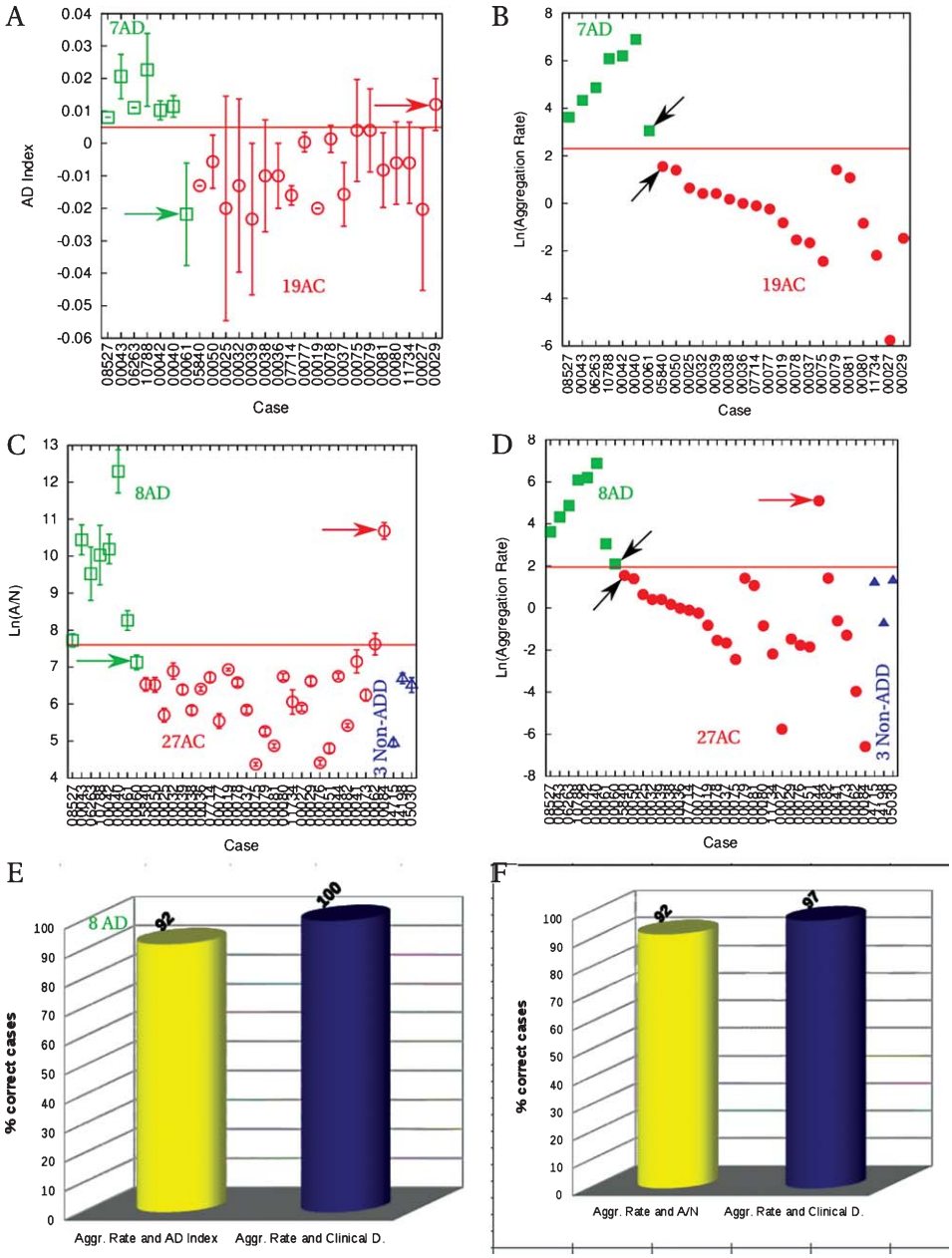

Fig. 6. Cross-validation of aggregation rate with the AD-Index and Morphology assay. A) AD-Index for each of the 26 cases is shown with the empty symbols. AD cases are in green and AC cases are in red. The two outliers (1 AD, 1 AC) are indicated by the green and red arrows respectively. Error-bars are standard errors of the mean (SEM). B) For the Morphology assay, the natural logarithm of the aggregation rate (filled symbols) is plotted for each of the same 26 cases as in panel A. Black arrows show the lowest AD value and the highest AC value. C) Ln (A/N) for each of the 38 cases is shown with the empty symbols. The two outliers (1 AD, 1 AC) are indicated by the green and red arrows, respectively. AD cases are in green, AC cases are in red, and Non-ADD cases are in blue. Error-bars are SEM. D) Natural logarithm of the aggregation rate (filled symbols) is plotted for each of the same 38 cases as in panel C. AD cases are in green, AC cases are in red, and Non-ADD cases are in blue. The horizontal lines in A-D represent the cut-off for the AD-Index, Ln (Aggregation Rate), and Ln (A/N). E) AD-Index cross-validates 92.3% of the 26 cases diagnosed with the aggregation rate in panel B (yellow bar). Aggregation rate for the 26 cases in panels A and B is 100% overlapping with the clinical diagnostic (blue bar). F) Ln (A/N) cross-validates 92.1% of the 35 cases diagnosed with the aggregation rate (yellow bar). Aggregation rate is 97% overlapping with the clinical diagnostic (blue bar).

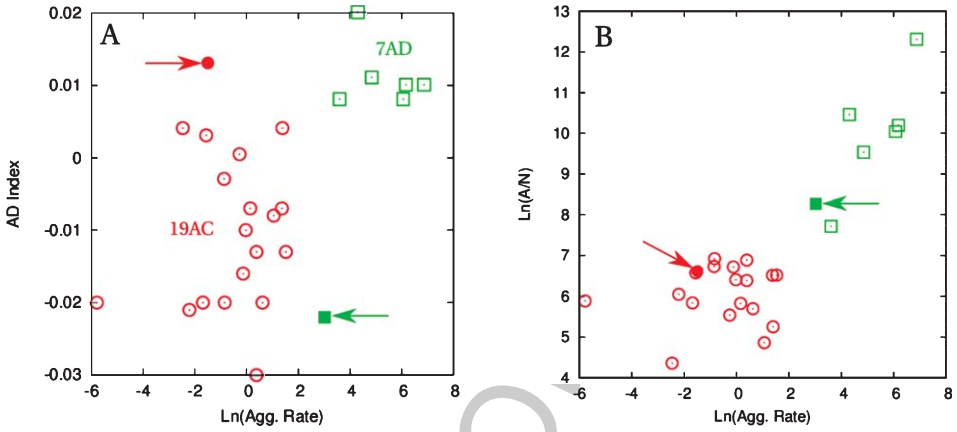

Fig. 7. A simple majority rule, i.e., 2 out of 3 assays give the same outcome, increases the agreement with clinical diagnosis to 100%. A) AD-Index versus the Ln (Aggregation Rate) reveals two cases, 1 AD (filled square and green arrow), 1 AC (filled circle and red arrow), as outliers for the AD-Index assay. B) The two outliers for the AD-Index are not outliers for the Morphology assay and Aggregation Rate, i.e., logarithm of the area per number of aggregates versus the logarithm of the aggregation rate. This makes 100% agreement with the clinical diagnostic.

Table 3
Quantification of the majority rule for the three biomarkers normalized by the cutoff values. The cutoff value is labeled as an uncertain (U) state

Sum of the normalized +1 values	Diagnosis
2, 3	Alzheimer's disease
0, 1	Age-matched control or Non Alzheimer's Disease dementia
2 or more cutoff values (U)	Not diagnosed

We have learned after systematic studies that applying boundary conditions for input variable in the assay such as number of cells/well, cell density/confluence (before using in the assay), days in culture (before using in the assay), disease duration, etc., has removed the outliers as well as the near cut-off cases (gray zone cases) in the A/N representation. However, in this data set of 38 cases we have not used such boundary conditions but used the more refined measure which is the aggregation rate (slope) instead.

Cross-validation

Cross-validation of the aggregation rate with the AD-Index

A comparison of the aggregation rate with a well-developed assay such as the AD-index [12–15] can also be a measure of the performance of this new biomarker. Out of the 38 cases tested with the aggregation rate assay, 26 were also tested with AD-Index assay western blot. Out of these 26 cases tested with both assays, 24 gave the same diagnosis (Fig. 6A, B). This represents 92.3% overlapping for the two biomarkers. As the AD-Index is a well developed and tested assay on more than 80% hyper-validated samples, we can consider it as a standard for the comparison with the aggregation rate. Furthermore, the AD-Index assay was improved by using Duolink (Olink) technology which offers a better dynamic range and a smaller variation for test-retest variation. Implicitly the AD-Index with Duolink (Olink) shows smaller errors than AD-Index western blot and increases the dynamic range. The aggregation rate agrees 100% with the clinical diagnosis for this population of 26 cases.

Cross-validation of the aggregation rate with the morphology assay

Furthermore we compare the aggregation rate with area per number of aggregates [5], which is also a well-studied assay. The results of this comparison can also be a measure of the performance of this new biomarker. All of the 38 cases tested with the aggregation rate were also tested for the simpler measure of A/N. Out of these 38 samples tested with both assays, 35 gave the same diagnosis (Fig. 6C, D). This represents 92.1% overlap for the two biomarkers. As A/N is a more developed and tested assay on more than 80% hyper-validated samples, we can consider it as a standard for the comparison with the aggregation rate. For this population of 38 cases, the aggregation rate agrees in 97% of the cases with the clinical diagnosis.

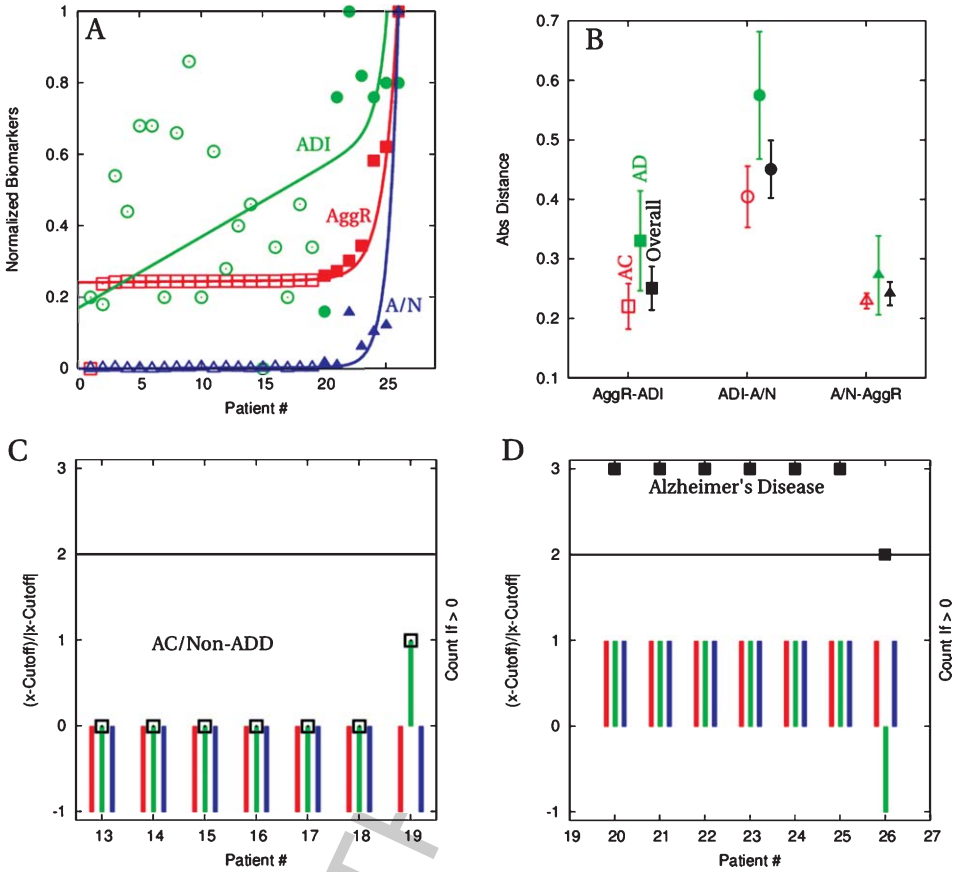

Fig. 8. Quantification of cross-validation. A) Aggregation Rate (AggR; red squares), AD-Index (ADI; green circles), and A/N(A/N; blue triangles) for 26 cases (19 AC, 7 AD) were normalized between 0 and 1. The age-matched control cases are represented by empty symbols and AD cases were represented by filled symbols. The solid curves are fits of the raw data (see the Methods section). B) Average distances between pairs of biomarkers, per group, are represented for AC in red, AD in green, and for the overall curves in black. The error-bars are standard errors of the means. C) Seven AC cases from panel A were normalized by the cutoff values for each biomarker as (x-Cutoff)/|x-Cutoff|. With red lines we represented the AggR, with green lines the ADI, and with blue lines the A/N. The possible output values for this cutoff normalization are 1 for AD, −1 for AC or uncertain (U) for cutoff values. The empty black squares on the right y scale represent the "count if >0" for the positive (+1) results of the biomarkers. If the results are 0 or 1 we accept that case as an age-matched control (AC) or Non-ADD. The cases 1 to 12 are the same as the cases 13 to 18. D) The seven AD cases are analyzed in the same way as in panel C. The filled black squares on the right y scale represent the "count if >0" for the positive (+1) results of the biomarkers. If the results are greater or equal with 2 then we accept the case as an AD case and this is the essence of the majority rule.

Importance of cross-validation

AD is a complex disease with a multifactorial structure in which many pathways are disrupted and/or affected. Furthermore the sporadic form of AD has an onset above 65 years old when the likelihood of co-morbidity with other diseases is very high. Therefore, a single biomarker will unlikely detect with high precision sporadic AD cases in their early progression when the drug efficacy for AD might be very high. The proposed biomarker quantifying the fibroblast aggregation rate, when cross-validated with other two more mature biomarkers, shows an overlap of approximately 92%. However, when considering the population of 26 cases tested with all three biomarkers and using a simple majority rule, i.e., 2/3 assays give the same result, the agreement with the clinical diagnosis increased to 100% (Fig. 7). Therefore, we believe that using more than one assay for diagnosing AD, as well as cross-validation using a majority rule, will help improve the rate of success for final diagnosis. The method of cross-validation of the three assays, presented here, can also increase the confidence of the clinical diagnosis.

Here we used the simple majority rule with reference to the clinical diagnosis. However, the same rule is expected to hold when used with reference to hyper-validated samples, i.e., autopsy confirmed AD and Non-ADD and non-demented AC.

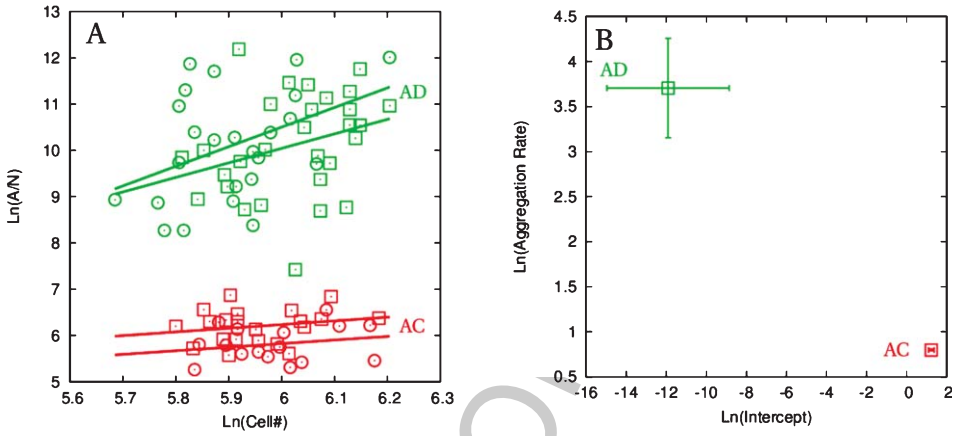

Fig. 9. Test-retest reliability for Aggregation rate. A) Ln (Aggregation Rate) versus Ln (Cell#) for 1 AD case in green and one age-matched controlled case in red. First experiments (circles) were repeated for the same cell lines with a different Matrigel lot (squares). Lines are the best fit. B) Ln (Aggregation Rate) versus the Ln (Intercept) for the two cases in panel A. Error-bars are the standard errors of the mean.

Quantification of cross-validation

In this section, we show a way to quantitatively measure the cross-validation for the three biomarkers discussed in this paper. For this purpose, we normalized the values of the three biomarkers for 26 patients, of which 19 were age-matched controls (AC) and 7 were AD (Fig. 8A). The normalized values were between 0 and 1 (please see the Methods section) and make the comparison between the three biomarkers easier. The AC cases are shown with empty symbols while the AD cases are shown with filled symbols. The AC cases show a linear dependence for all three biomarkers, and it is almost flat for aggregation rate and A/N. The AD cases show a highly nonlinear dependence for which we used an exponential curve to fit. In Fig. 8A, the aggregation rate (AggR) values were ranked from minimum, 0, to maximum 1. The AD-Index biomarker (green circles in Fig. 8A) show a significant noise especially for the AC cases.

To measure the closeness of the three biomarkers, we chose to look at the absolute difference between pairs of values on the case by case basis (see the Methods section and Fig. 8B). By far the less noisy difference is |A/N-AggR|. Probably the noise of the other two absolute differences, |AggR-ADI| and |ADI-A/N|, comes from the noise in the AD-Index.

An overview of the closeness of the three biomarkers is represented in Fig. 8B where the average of the absolute distances is presented for the AC cases (red squares), AD cases (green squares), and overall cases (black squares). The absolute differences between the AD cases (green) are bigger than the absolute differences between the AC cases, while the overall absolute difference is in between. Again the absolute difference between the A/N and aggregation rate, |A/N-AggR|, is the smallest suggesting that the two biomarker measures have the strongest correlation.

Finally we show a way of quantifying the majority rule for the three biomarkers we discussed in this paper. The same majority-rule method could be applied to more than three biomarkers. For the purpose of discussing the method, we used the three biomarker values for the 7 AC and 7 AD patients and normalized these values as $\frac{(x-Cutoff)}{|x-Cutoff|}$ (see the Methods section), where x is the current value of the biomarker and the Cutoff is the separation between the AC and AD groups. The cutoff values are determined at the intersection of the two Gaussian distributions fitting the AC and AD data. The normalized values as described above can have one of the three possible states: -1 for AC and Non-ADD, 1 for AD, or uncertain (U) for the cutoff value. The normalized AD values for the three AD biomarkers are shown in Fig. 8D with color bars. With red lines, we represented the AggR, with green lines the ADI, and with blue lines the A/N. For cases 19 and 26, one biomarker (AD-Index in green) is giving a normalized value opposite to the other two biomarkers. Therefore these cases are diagnosed correctly if we follow the majority rule. One way to quantify this rule is to sum up all the +1 values/per case using the simple function like count if (>0) as shown by the empty black squares in Fig. 8C or filled black squares in Fig. 8D (see the Methods section). If the result of the "count if" is greater or equal than 2, then the case is an AD (Fig. 8D). If the result of the count if is less than 2, than that case is an AC/Non-ADD case (Fig. 8C). If two or more biomarkers for one case have the cutoff value (U), then we cannot diagnose that case on the

basis of these three biomarkers. Similarly one can use the count if (<0) which is a redundant pathway. This approach is summarized in Tables 2 and 3 and Fig. 8C and D.

Test–retest reliability

The test retest reliability was verified for the Aggregation Rate with two cells lines (1 AC, 1 AD) (Fig. 9). First experiments (circles) were repeated for the same cell lines with a different Matrigel lot. Lines are the best fit. The average values for the Ln (Aggregation Rate) and Ln (Intercept) are presented in Fig. 9B, and the error-bars represent the standard error of the mean.

CONCLUSIONS

In summary, the slope intercept representation of the human skin fibroblast aggregation showed significant separation in the slope but not in the intercept. This suggests that the elevated rate of change of cell aggregation with increasing cell density in AD is the driving force for this new biomarker.

Analyses on 38 cases, out of which 9 were banked cases and 29 were cases from the clinic, suggest a clear separation between AD and AC/Non-ADD when using the aggregation rate (slope) as a biomarker.

The analysis of the probability distributions of the slope and intercept for 35 samples suggests that the probability distribution for the AC group ($n = 27$) is narrower and resides on the tail of the probability distribution of the AD group ($n = 8$) which is wider. This suggests that for larger data sets, the estimated overlapping probability for the two groups, AD and AC, is less than 10%.

Furthermore the trend of higher aggregation rate for AD cases when compared with AC/Non-ADD cases is in line with our previous studies and reports showing that AD cells are consistently less adhesive than the AC/Non-ADD cells [5]. The abnormal fibroblast aggregation rate in AD is similar with the abnormal fibroblast aggregation in Down syndrome [7] or in DMD [6, 8].

The new biomarker, aggregation rate (A), was cross-validated with two more mature assays, AD-Index (B) and A/N (C). The cross-validation resulted in 92% overlap with each of the assays and in >97% overlap with the clinical diagnosis. The 92% agreement of the new biomarker, A, with the two more mature biomarkers, B, and C, which were also tested with hyper-validated samples makes this new biomarker, via Euclid's common notions [17], a hyper-validated biomarker. In a more concise form, if biomarkers B, C = hyper-validated and if B, C = A (92%) then A = hyper-validated (92%).

Furthermore we show here for the first time that a simple majority rule, i.e., when two out of the three diagnostic assays agree, they also agree with clinical diagnosis 100%. We expect this majority rule to yield the same high level of agreement with autopsy-confirmed/genetically determined (hyper-validated) samples.

ACKNOWLEDGMENTS

We would like to thank Dr. Camilla Forssten and Dr. Gerhard Nebe-von-Caron from Alere Inc. for their ongoing valuable discussions and Alere Diagnostic for their alliance support. Finally, we would appreciate Dr. Shirley Neitch from Marshall University, Huntington, WV, for her oversight and the clinical diagnosis for the 29 fresh samples presented in this study.

Authors' disclosures available online (http://www.j-alz.com/disclosures/view.php?id=2330).

SUPPLEMENTARY MATERIAL

The supplementary tables are available in the electronic version of this article: http://dx.doi.org/10.3233/JAD-140672.

REFERENCES

[1] Zhao WQ, Ravindranath L, Mohamed AS, Zohar O, Chen CH, Lyketsos CG, Etcheberrigaray R, Alkon DL (2002) MAP kinase signaling cascade dysfunction specific to Alzheimer's disease in fibroblasts. *Neurobiol Dis* **11**, 166-183.

[2] Khan TK, Alkon DL (2006) An internally controlled peripheral biomarker for Alzheimer's disease: Erk1 and Erk2 responses to the inflammatory signal bradykinin. *Proc Natl Acad Sci U S A* **103**, 13203-13207.

[3] Khan TK, Alkon DL (2008) Early diagnostic accuracy and pathophysiologic relevance of an autopsy-confirmed Alzheimer's disease peripheral biomarker. *Neurobiol Aging* **31**, 889-900.

[4] Khan TK, Nelson TJ, Verma VA, Wender PA, Alkon DL (2009) A cellular model of Alzheimer's disease therapeutic efficacy: PKC activation reverses Abeta-induced biomarker abnormality on cultured fibroblasts. *Neurobiol Dis* **34**, 332-339.

[5] Chirila FV, Khan TK, Alkon DL (2013) Spatiotemporal complexity of fibroblast networks screens for Alzheimer's disease. *J Alzheimers Dis* **33**, 165-176.

[6] Hillier J, Jones GE, Statham HE, Witkowski JA, Dubowitz V (1985) Cell surface abnormality in clones of skin fibroblasts from a carrier of Duchenne muscular dystrophy. *J Med Genetics* **22**, 100-103.

[7] Wright TC, Orkin RW, Destrempes M, Kurnit DM (1984). Increased adhesiveness of Down syndrome fetal

fibroblasts *in vitro*. *Proc Natl Acad Sci U S A* **81**, 2426-2430.

[8] Jones GE, Witkowski JA (1981) Analysis of skin fibroblast aggregation in Duchenne muscular dystrophy. *J Cell Sci* **48**, 291-300.

[9] Whur P, Koppel H, Urquhart C, Williams DC (1977) Quantitative electronic analysis of normal and transformed BHK21 fibroblast aggregation. *J Cell Sci* **23**, 193-209.

[10] Swift DL, Friedlander SK (1964) The coagulation of hydrosols by Brownian motion and laminar shear flow. *J Colloid Sci* **19**, 621-647.

[11] Bikfalvi A, Cramer EM, Tenza D, Tobelem G (1991) Phenotypic modulations of human umbilical vein endothelial cells and human dermal fibroblasts using two angiogenic assays. *Biol Cell* **72**, 275-278.

[12] Hadley MA, Byers SW, Suarez-Quian CA, Kleinman HK, Dym M (1985) Extracellular matrix regulates Sertoli cell differentiation, testicular cord formation and germ cell development. *J Cell Biol* **101**, 1511-1522.

[13] Ingber D, Folkman J (1989) Mechanochemical switching between growth and differentiation during fibroblast growth factor-stimulated angiogenesis *in vitro*. Role of extracellular matrix. *J Cell Biol* **109**, 317-331.

[14] Furukawa KS, Ushida T, Sakai Y, Kunii K, Suzuki M, Tanaka J, Tateishi T (2001) Tissue-engineered skin using aggregates of normal human skin fibroblasts and biodegradable material. *J Artif Organs* **4**, 353-356.

[15] Furukawa KS, Ushida T, Sakai Y, Suzuki M, Tanaka J, Tateishi T (2001) Formation of human fibroblast aggregates (spheroids) by rotational culture. *Cell Transplantation* **10**, 441-445.

[16] Dai W, Saltzman WM (1996) Fibroblast aggregation by suspension with conjugates of poly(ethy1ene glycol) and RGD. *Biotechnol Bioeng* **50**, 349-356.

[17] Euclid (2006) *Elements: Books I-XIII-Complete and Unabridged*, Translated by Sir Thomas Heath. Barnes and Noble.